

# Polarimetric Interferometry – Remote Sensing Applications

Martin Hellmann<sup>1</sup>, Shane R. Cloude<sup>2</sup>

<sup>1</sup>German Aerospace Center (DLR), VO-ST, Linder Höhe, D-51140 Köln, Germany,  
e-mail: [martin.hellmann@dlr.de](mailto:martin.hellmann@dlr.de)

<sup>2</sup>Shane R Cloude, e-mail: [scloude@ieee.org](mailto:scloude@ieee.org)

## INTRODUCTION

This lecture is mainly based on the work of S.R. Cloude and presents examples for remote sensing applications Polarimetric SAR Interferometry (PolInSAR). PolInSAR has its origins in remote sensing and was first developed for applications in 1997 using SIRC L-Band data [1,2]. In its original form it involved generating phase differences between interferograms formed using different polarization combinations. Later these phase differences were observed to be correlated with vegetation height [2]. However, it was quickly realized that more accurate estimates of height could be obtained by correcting the phase differences using coherent wave scattering models [3,4,6]. Since then there have been several groups working on the development and inversion of suitable models for the interpretation of POLInSAR data. A particularly useful model, which presents a good compromise between physical structure and model complexity is a variant of that first developed by Treuhaft et al [3,4]. This 2-layer model is widely used in interferometric SAR (InSAR) applications. Here we review its main structure and importance in POLInSAR.

In case of polarimetric interferometry we get two fully polarimetric measurements from both ends of the interferometric baseline and therefore, 2 S-matrices [ $S^1$ ] and [ $S^2$ ].

From these measurements we can derive the basic radar observable in POLInSAR, the 6x6 coherency matrix of a pixel, defined as shown in equation 1

$$\langle \underline{k} \cdot \underline{k}^{*T} \rangle = \begin{bmatrix} T_{11} & \Omega_{12} \\ \Omega_{12}^{*T} & T_{22} \end{bmatrix} \quad (1)$$

$$\underline{k} = \frac{1}{\sqrt{2}} \begin{bmatrix} S_{hh}^1 + S_{vv}^1 & S_{hh}^1 - S_{vv}^1 & 2S_{hv}^1 & S_{hh}^2 + S_{vv}^2 & S_{hh}^2 - S_{vv}^2 & 2S_{hv}^2 \end{bmatrix}^T$$

where superscripts 1 and 2 denote measurements at the two ends of the baseline and  $\langle \cdot \rangle$  represents ensemble averaging. We can partition the matrix into 4 3x3 submatrices, the two polarimetric coherency matrices  $T_{ii}$  and the 2 polarimetric interferometry matrices  $\Omega_{ii}$ . Generally this matrix must be estimated by multi-look processing of the data using a local window centred on the pixel of interest. Consequently, full matrix estimation follows a complex Wishart distribution and this enables characterisation of the fluctuation statistics in POLInSAR data [5].

According to the 2-layer vegetation model, first derived by Treuhaft [4] and extended for fully polarimetric interpretation by Papathanassiou [6], the complex interferometric coherence for a random volume over a ground can be derived as shown in equation 2 and shown schematically in figure 1

Hellmann, M.; Cloude, S.R. (2007) Polarimetric Interferometry – Remote Sensing Applications. In *Radar Polarimetry and Interferometry* (pp. 9-1 – 9-22). Educational Notes RTO-EN-SET-081bis, Paper 9. Neuilly-sur-Seine, France: RTO.  
Available from: <http://www.rto.nato.int/abstracts.asp>.

$$\tilde{\gamma} = \frac{\underline{w}^{*T} \Omega_{12} \underline{w}}{\underline{w}^{*T} T_{11} \underline{w}} \quad (2)$$

$$T_{11} = I_1^V + e^{-\frac{2\sigma h_v}{\cos \theta_o}} I_1^G \quad \Omega_{12} = e^{i\phi_2} I_2^V + e^{i\phi_1} e^{-\frac{2\sigma h_v}{\cos \theta_o}} I_2^G$$

$$I_1^V = e^{-\frac{2\sigma h_v}{\cos \theta}} \int_0^{h_v} e^{\frac{2\sigma z'}{\cos \theta_o}} T_V dz' \quad I_1^G = \int_0^{h_v} \delta(z') e^{\frac{2\sigma z'}{\cos \theta_o}} T_g dz' = T_g$$

$$I_2^V = e^{-\frac{2\sigma h_v}{\cos \theta}} \int_0^{h_v} e^{\frac{2\sigma z'}{\cos \theta_o}} e^{ik_z z'} T_V dz' \quad I_2^G = T_g$$

where  $\underline{w}$  is a 3 component unitary complex vector defining the choice of polarization [2],  $\sigma$  the mean wave extinction in the medium,  $k_z$  the vertical wavenumber of the interferometer (following spectral range filtering) and  $\theta$  the mean angle of incidence. The angles  $\phi_1$  and  $\phi_2$  are the phase centres of the bottom of layers 1 and 2 respectively.

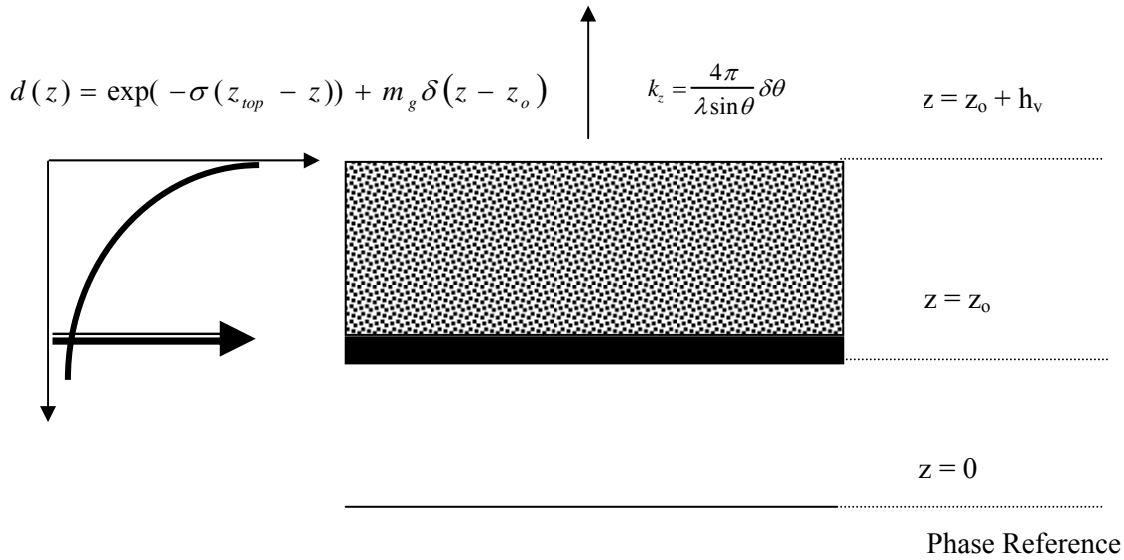


Figure 1: Schematic representation of the 2-Layer coherence model for vegetated land surfaces [3]

$T_V$  is the 3 x 3 diagonal coherency matrix for the volume scattering and  $T_g$  the reflection symmetric ground scattering coherency matrix, defined as shown in equation 3 [6]

$$T_V = m_v \begin{bmatrix} 1 & 0 & 0 \\ 0 & \mu & 0 \\ 0 & 0 & \mu \end{bmatrix} \quad 0 \leq \mu \leq 0.5 \quad T_g = m_g \begin{bmatrix} 1 & t_{12} & 0 \\ t_{12}^* & t_{22} & 0 \\ 0 & 0 & t_{33} \end{bmatrix} \quad (3)$$

This two-layer model is supported by radar tomographic experiments at L-band [7,8] and shows that  $\langle |2*HV| \rangle^2 = \langle |HH-VV| \rangle^2$  as expected for the random volume assumption in figure 1 and  $T_v$  in equation 3. This supports the use of a random rather than an oriented volume for L-band forest remote sensing.

Further, by assuming that the canopy extends from crown to ground then we can simplify equation 2 by setting  $\phi_1=\phi_2$ . Later we shall examine the consequences of this assumption, but for the moment we assume the bottom of the canopy corresponds to the ground surface.

By combining equations 2 and 3 we obtain the following explicit equation for the complex coherence

$$\tilde{\gamma} = \frac{\underline{w}^{*T} (e^{i\phi_1} I_2^V + e^{\frac{2\sigma h_v}{\cos\theta_o}} T_g e^{i\phi_1}) \underline{w}}{\underline{w}^{*T} (I_1^V + e^{\frac{2\sigma h_v}{\cos\theta_o}} T_g) \underline{w}} = \frac{\underline{w}^{*T} (e^{i\phi_1} v^{-1} I_2^V + e^{i\phi_1} v^{-1} T_g) \underline{w}}{1 + \underline{w}^{*T} v^{-1} T_g \underline{w}} \quad v^{-1} = \frac{1}{\underline{w}^{*T} I_1^V \underline{w}} \quad (4)$$

which can be rewritten as the equation of a straight line in the complex plane as

$$\hat{\gamma}(\underline{w}) = e^{i\phi_1} \frac{\hat{\gamma}_v + \mu(\underline{w})}{1 + \mu(\underline{w})} = e^{i\phi_1} \left( \hat{\gamma}_v + \frac{\mu(\underline{w})}{1 + \mu(\underline{w})} (1 - \hat{\gamma}_v) \right) = e^{i\phi_1} (\hat{\gamma}_v + L(\underline{w})(1 - \hat{\gamma}_v)) \quad 0 \leq L(\underline{w}) \leq 1 \quad (5)$$

where the ground-to-volume scattering ratio  $\mu$  includes the effects of wave extinction in the medium and is defined as

$$\mu(\underline{w}) = \frac{2\sigma}{\cos\theta_o (e^{\frac{2\sigma h_v}{\cos\theta_o}} - 1)} \frac{\underline{w}^{*T} T_g \underline{w}}{\underline{w}^{*T} T_v \underline{w}} \geq 0 \quad (6)$$

Note that  $\mu$  is positive semi-definite and that the max/min values of this function versus polarization are given by the eigenvalues of a contrast optimization problem since

$$\max_{\underline{w}} \frac{\underline{w}^{*T} T_B \underline{w}}{\underline{w}^{*T} T_A \underline{w}} \Rightarrow T_A^{-1} T_B \underline{w}_{opt} = \mu \underline{w}_{opt} \quad (7)$$

The eigenvalues  $\mu_i$  are non-degenerate, due to the strong polarization dependence of ground scattering, and this lends support to the variation of coherence with polarization in equation 4. We note that the three eigenvectors of this problem are not mutually orthogonal. This is in contrast to the situation when differential propagation effects are important, when the optimum  $w$  vectors are related to the propagation eigenpolarisations, which for a single vegetation layer are mutually orthogonal [10,11]. Note also that for a reflection symmetric ground with azimuthally symmetric vegetation cover (as implied by equation 3), the minimum eigenvalue will be obtained for the HV channel. In the more general case, the coherence optimizer [1,2] can be used to find the max and min ground components in equation 6.

Consequently, in equation 5 only  $\mu$  is a function of polarisation. This arises since  $\gamma_v$  is a polarization independent volume integral as shown in equation 8.

$$\hat{\gamma}_v = \frac{\underline{w}^{*T} \int_0^{h_v} e^{\frac{2\sigma z'}{\cos\theta_o}} e^{ik_z z'} T_v dz' \underline{w}}{\underline{w}^{*T} \int_0^{h_v} e^{\frac{2\sigma z'}{\cos\theta_o}} T_v dz' \underline{w}} = \frac{m_v \int_0^{h_v} e^{\frac{2\sigma z'}{\cos\theta_o}} e^{ik_z z'} dz'}{m_v \int_0^{h_v} e^{\frac{2\sigma z'}{\cos\theta_o}} dz'} = \frac{2\sigma}{\cos\theta_o (e^{2\sigma h_v / \cos\theta_o} - 1)} \int_0^{h_v} e^{ik_z z'} e^{\frac{2\sigma z'}{\cos\theta_o}} dz' \quad (8)$$

In the limit that the wave extinction is zero this reduces to an elementary sinc function. Figure 2 shows how the volume coherence varies as a function of vegetation height and extinction for a vertical wavenumber  $kz = 0.2$  (corresponding to a 20m baseline at L band for the DLR E-SAR airborne system. Note that the coherence falls with increasing vegetation height as a consequence of volume decorrelation. However, the effect of unknown extinction makes the relationship between coherence and height ambiguous.

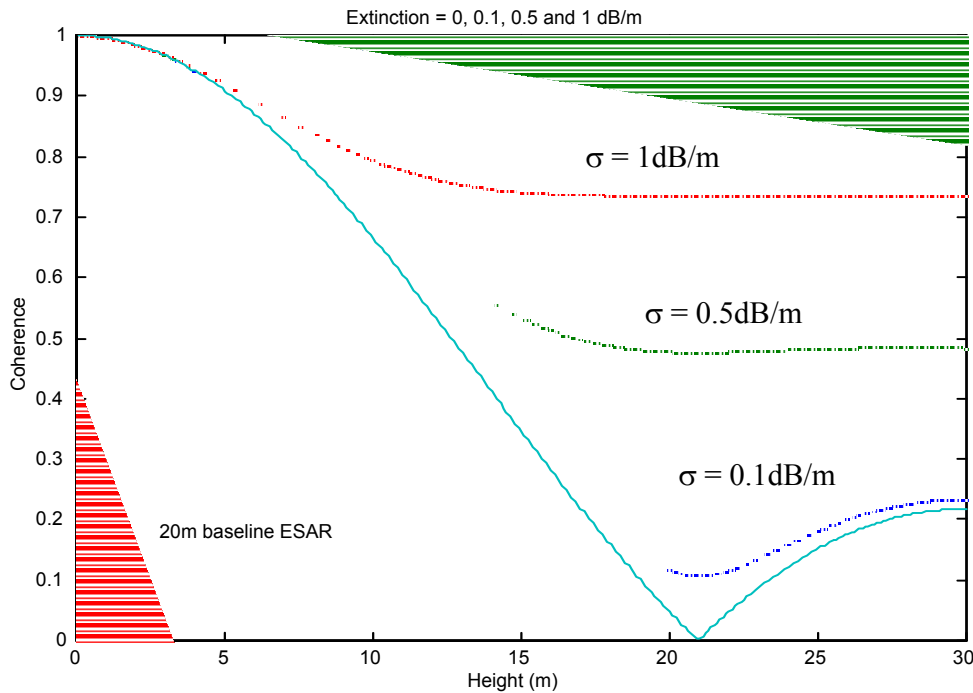


Figure 2: Coherence variation versus tree height and mean extinction [Cloude]

As well as the coherence amplitude, consideration must also be given to variation of the phase of the observed interferogram. According to equation 8, the presence of vegetation causes an offset in the estimation of the interferometric phase of the ground topography given by half the vegetation height (or more as the extinction increases). This offset decreases with increasing ground component but is always present, biasing the estimation of ground topography. Note that the above vegetation-plus-ground scattering model makes no restrictions about the observed phase difference between the elements of a single scattering matrix. These relative polarimetric phase differences are caused by a polarisation dependent scattering phase term introduced by the scatterer and cancel each other when an interferogram is formed by using the same polarisation at both ends of the baseline. This is not the case when the interferogram is formed by using different polarisations at either end of the baseline. In this case topographic and scattering related coherence and phase information is mixed. Hence care is required to distinguish the polarimetric interferometric and polarimetric phase angles. This distinction was overlooked in [9], where the authors proposed a relationship between these two phase angles which has only limited validity.

Inversion of equation 5 is greatly facilitated by employing a geometrical interpretation inside the unit circle of the complex coherence plane. Figure 3 shows how the model maps coherence points from equation 5 onto a line in the complex plane. This line has three important features:

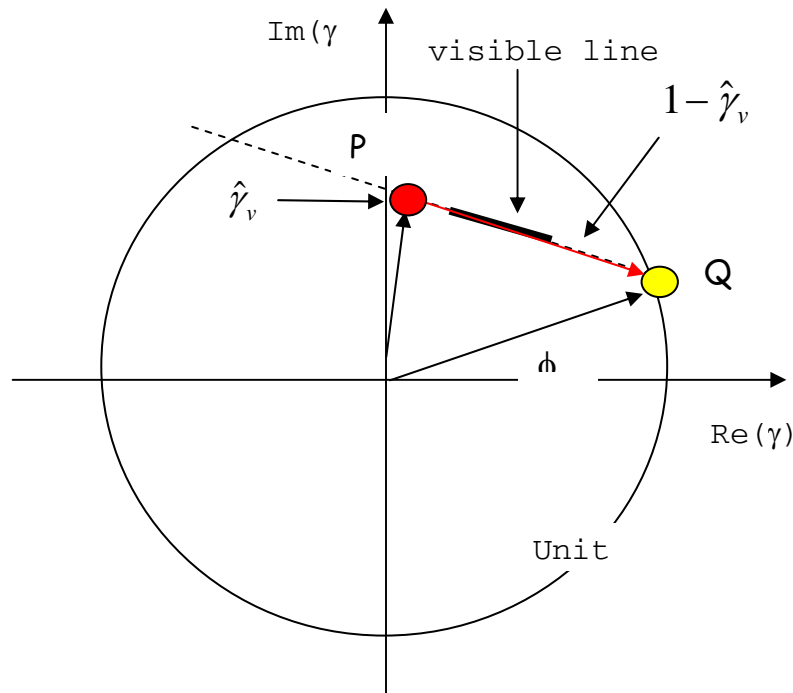


Figure 3: The line model for polarimetric variation of interferometric coherence

- 1) The line intersects the circle at 2 points. One of these is the underlying topography related phase (shown as the point Q in figure 3). The other is a false solution and must be rejected by the inversion process
- 2) The volume coherence  $\gamma_{\text{v}}$  lies at one end of the line ( $\mu=0$ ). It is shown as the point P in figure 2. This point is central to the estimation of height and extinction and needs to be estimated from the data.
- 3) The visible length of the line in the data may only be a fraction of PQ and neither P nor Q may be directly observed. The visible length depends on baseline, operating frequency and vegetation density [6]. However the line can be extrapolated to enable parameter estimation as we now show.

### POLINSAR MODEL INVERSION

Inversion of equation 5 involves taking observations of the complex coherence at a number of different polarizations and then minimizing the difference between the model predictions and observations in a least squares sense. In most previous studies [6] this has been implemented as a six-dimensional optimisation problem using standard iterative procedures. Due to the non-linear nature of the optimisation problem, the obtained solution depends strongly on the choice of the starting values. Poor starting values may lead to ambiguous and/or unstable parameter estimates [15,17,18,19]. However, we can clarify the requirements of the inversion by breaking the process down into three separate stages as follows:

**Stage 1 : Least Squares Line Fit**

The first stage is to find the best-fit straight line inside the unit circle of interferometric coherence. To do this we vary two phase variable  $\psi_1$  and  $\psi_2$  as shown in figure 5.

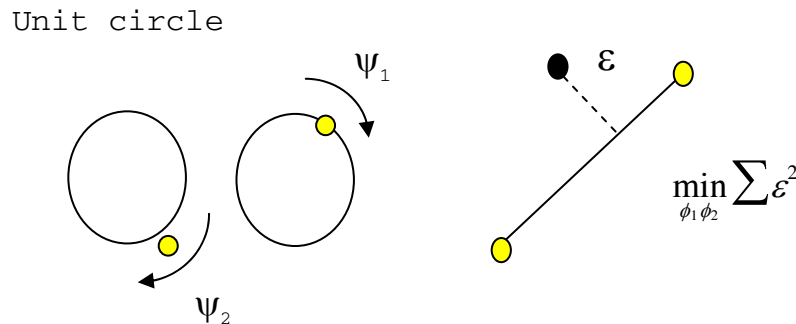


Figure 4: Phase-based least square line fit

Each pair defines a line and we choose the pair that minimises the MSE between the line and set of coherence points as shown. One way to do this is to use a total least squares line fit to the real and imaginary components of the data and then use the line parameter estimates to secure the intersection points. Alternatively a faster least squares line fit in the real and/or imaginary parts can secure an estimate of the minimum error solution [14]. An alternative method based on a maximum likelihood approach using the complex Wishart distribution has recently been outlined in [21]. Phase centre estimation based on the ESPRIT processing technique has also been employed for this purpose [22].

In either case, this process requires some care in complex coherence estimation. Problems can arise with:

1) Phase and Coherence fluctuations. The Cramer-Rao bounds on variance of these two parameters can be approximated as [12]

$$\text{var}_{\phi} > \frac{1-|\gamma|^2}{2N|\gamma|^2} \quad \text{var}_{\gamma} > \frac{(1-|\gamma|^2)^2}{2N} \tag{9}$$

where N is the number of looks. Hence N needs to be high enough to secure good estimates at the lowest coherence expected along the line. The fluctuations should be small compared to the visible length of the line. To this end the coherence maximiser helps [2] as it secures the highest possible coherence values and hence the smallest CR bounds. Care is also required when speckle filtering the data to ensure that no distortion of polarimetric information occurs, as recently demonstrated in [23]

2) Coherence bias for low coherence values. Standard boxcar methods overestimate low coherence values and hence distort the line parameters [13]. Either unbiased estimators should be used or the interferometer design should avoid low values of coherence through judicious choice of the baseline. The bias reduces with increasing coherence and with increasing N.

3) SNR variations can cause loss of coherence, again distorting the line. This is a potentially serious issue as SNR is generally a function of polarisation. Fortunately, such variations are seen mainly in surface scattering and light vegetation cover and not in forestry applications.

4) Temporal decorrelation. In repeat-pass systems, coherence can fall due to changes in the scene between passes. To avoid this, single pass polarimetric interferometry is preferred. We note from equation 1 that volume temporal decorrelation effects will not necessarily destroy the line structure, only lower the coherence so causing additional problems through 1) and 2) above. For example, in the presence of wind driven vegetation decorrelation, only the coherent volume integral factor  $I_2^V$  in equation 2 is modified. The effect is to reduce the coherence magnitude without changing the phase of the integral. This can be modelled as a multiplicative scalar factor  $\gamma_t$ , the temporal decorrelation and equation 5 must then be modified as shown in equation 10

This remains the equation of a straight line and both  $\phi$  and  $\mu$  are invariant to such transformations. However the height/extinction estimation becomes ambiguous. Regularisation of the solution can be

$$\tilde{\gamma} = e^{i\phi} \left( \gamma_t \tilde{\gamma}_v - \frac{\mu}{1 + \mu} (1 - \gamma_t \tilde{\gamma}_v) \right) \quad (10)$$

achieved by assuming a fixed value for the mean extinction, as we show later. A second problem is that the coherence values decrease and this increases the variance of the phase/coherence estimates according to equation 9.

5) Even if all other factors 1-4 are minimised, the line model assumption may not be correct. This can arise for several reasons, such as when the vegetation becomes oriented and we have differential extinction and propagation phase. In this case the volume coherence itself becomes a function of polarisation. A suitable statistical confidence test for the line can be applied as shown in [14]. Oriented volume effects can also be identified through the presence of orthogonal eigenvectors and the rank order of the coherence values. [10,11]. Recently a technique for determining the coherence region shape has been developed [20] although in its current form it takes no account of the intrinsic statistical fluctuations in interferometric coherence and phase data. The output from stage 1 is then a set of  $\psi_1, \psi_2$  for each pixel. The next stage involves deciding which of these is the true ground phase through the process of vegetation bias removal.

**Stage 2 : Vegetation Bias Removal**

In the second stage we must choose one of the pair  $\psi_1, \psi_2$  as the underlying ground topographic phase for each pixel. To do this we extract the line from figure 4 and mark the polarization states in rank order as shown schematically in figure 6. It follows from equation 4 that the ground-to-volume ratio  $\mu$  is given by the distance along the line as shown in figure 5. We see that the nearer a coherence point is to Q, the higher is the corresponding ground-to-volume ratio  $\mu$ .

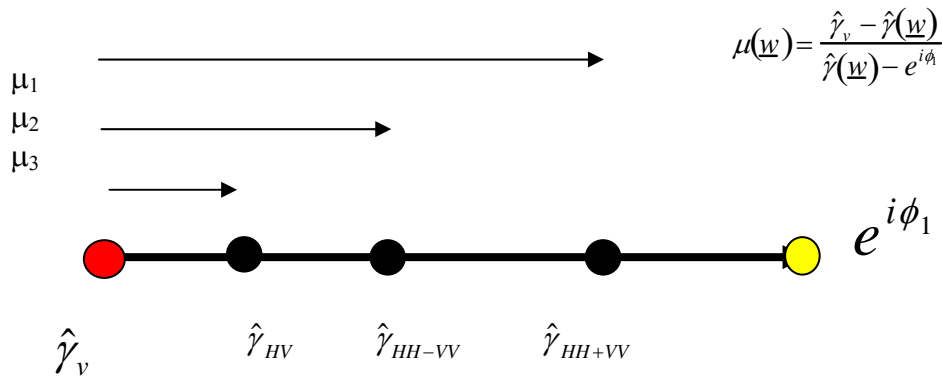


Figure 5: Relative location of polarisation states along the coherence line

While HH+VV and HH-VV can change relative position depending on whether direct ground or dihedral effects are dominant, it is very unlikely that the strongest ground-to-volume component will arise in the HV channel. This is based on scattering physics, which indicates that dihedral effects in vegetation generally lie orthogonal to HV [26], direct ground backscatter at L band has only a weak HV signal while canopy scattering has a strong HV signal. Hence it is reasonable to expect that the HV coherence channel will be ranked furthest away in distance from the true ground phase point Q (see figure 2 for experimental validation). Again some care is required, as statistical fluctuations can change the rank order and so statistical significance tests are again required.

Nevertheless, this gives us a systematic way of breaking the symmetry between the two points  $\psi_1, \psi_2$ , of deciding on the likely ground phase point and of applying the appropriate inversion model (random volume plus ground or oriented volume for example). Using this procedure we can now select the appropriate model and generate an interferogram, the phase of which,  $\phi$  corresponds directly to the true ground topography estimate. Note that this can be achieved through a combination of line fitting and rank ordering of coherence, both of which are fast processes to compute. As an alternative strategy to bias removal, the two points can initially be kept and each used in a stage 3 height estimation procedure (see below). As long as the tree height is less than the  $\pi$  height of the interferometer, then only one point will yield a good model fit thus enabling bias removal to be undertaken in stage 3. This provides a better quantitative approach but incurs the extra overhead of having to solve the model twice instead of only once for each point.



### Stage 3 : Height and Extinction estimation

To estimate the two remaining parameters, height and extinction, we use the estimate of ground phase  $\phi$  together with equation 8 to find the intersection point between the coherence line and the curve corresponding to the height/extinction variations. Figure 6 demonstrates the geometry of this intersection process. The ground phase in this simulation lies at zero degrees and we show 3 simulated coherence values along the line. By fixing  $\sigma$  at two different values and then varying the height, we obtain two coherence loci as shown. Where the curve intersects the line we have a candidate  $\gamma_{\text{v}}$  point.

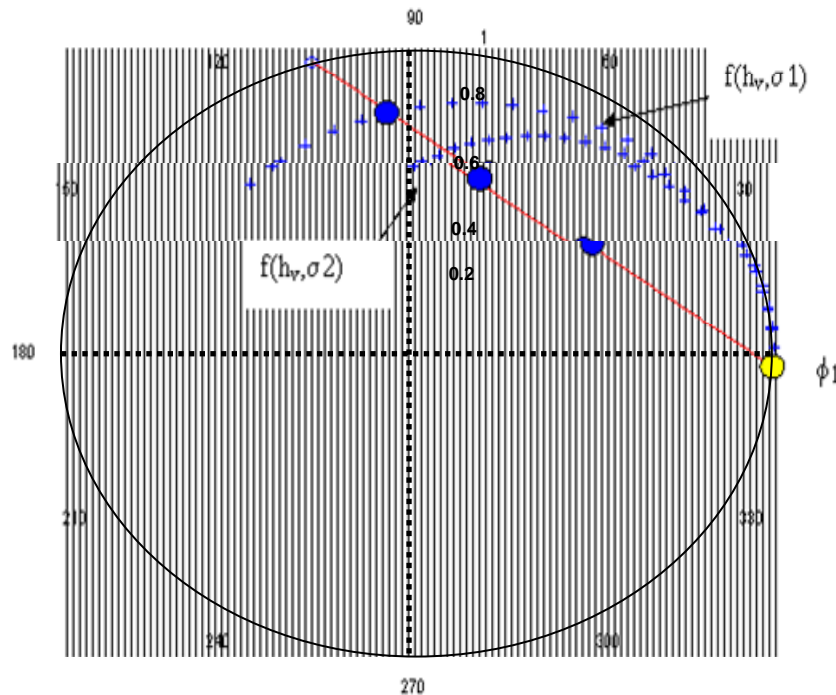


Figure 6 Geometrical interpretation of height and extinction estimation

We show two such intersections, one of which crosses the line to split the observed coherence values. This cannot be a physical solution, as it generates negative  $\mu$ , which from equation 6 is not possible. We must therefore take as the first candidate solution, parameters which cause the curve to intersect the line at the observed coherence value furthest from  $\phi$  (upper curve in figure 6).

This ensures non-negative ground scattering components for all observed polarizations but makes the assumption that for the intersection coherence point, the ground-to-volume scattering ratio  $\mu$  is zero. This point then becomes our estimate of  $\gamma_{\text{v}}$ . Hence unambiguous height/extinction estimation with single baseline polarimetric interferometry requires that  $\gamma_{\text{v}}$  be observed in the data.

The robustness of the height inversion process then rests on this assumption. The basic problem arises because all intersection points beyond the furthest coherence are also valid solutions for the volume coherence (figure 8). They represent height/extinction combinations that yield a volume coherence which both satisfies the model of equation 5 and the observed data. Note however that  $\gamma_{\text{v}}$  must itself lie on the line and hence the ambiguous solutions are also constrained to this line. This is an important observation, as from figure 5 the multiple solutions represent monotonically increasing ground contribution with distance along the line (figure 7).

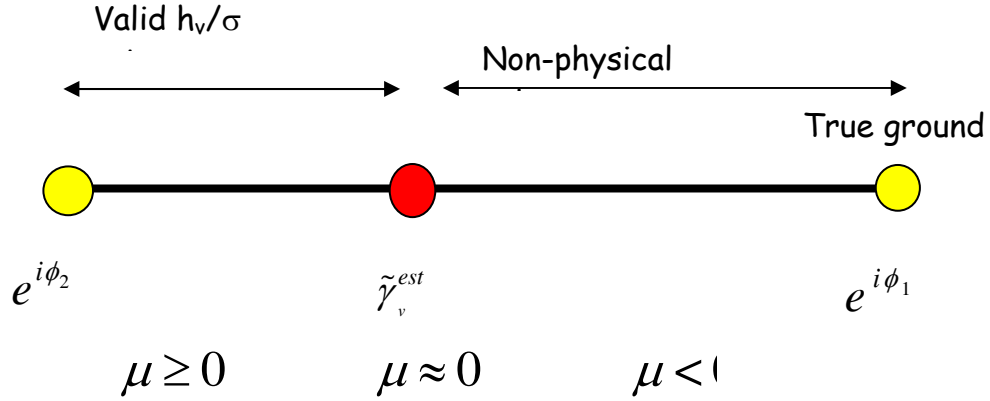


Figure 7: Line model ambiguity region

This permits us to regularize the solution by making assumptions about the minimum ground-to-volume ratio in the data. This ambiguity region has also been noted in [15,19] although in [19] a different regularization approach was employed. Note that since we know the phase point  $\phi$  from stage 2, we can easily locate the furthest coherence point in the data. This becomes our estimate of the volume coherence  $\hat{\gamma}_{est}$ . From the baseline data we can estimate  $k_z$  and then pre-calculate a look-up table (LUT) of  $\gamma_w$  as a function of  $h_v$  and  $\sigma$  using equation 8. By comparing  $\hat{\gamma}_{est}e^{-i\phi}$  with the LUT, we can then secure estimates of the height and extinction without the need for iterative optimization algorithms. Simulations have shown that in order to secure around 10% height accuracy, the minimum ground-to-volume scattering ratio needs to be less than -10dB [27]. From the symmetry assumptions in equation 3 it follows that the HV channel will most often satisfy this requirement and hence cross polarization measurements are very important for reliable height estimation.

### 1.2.1 The Effect of Temporal Decorrelation on Height/Extinction estimation

We now consider how the above algorithm for height/extinction estimation must be modified in the case of repeat pass systems when temporal decorrelation becomes an important issue. Equation 10 shows that the line model is still valid and hence the line fit and ground phase estimation procedures are unchanged. However, the effect of temporal decorrelation is to make the coherence amplitude too small for the observed vegetation bias  $\phi_w$ . This is shown as the dotted line in figure 8. The true volume coherence is shifted radially to the origin by the temporal decorrelation and so the geometrical effect is to rotate and stretch the line about the unit circle ground phase point as shown in figure 7.

Hence there will no longer be an intersection between the height/extinction curve and the observed volume coherence point, as in figure 7. To secure a solution we must therefore move the observed volume coherence point radially in the coherence plane to compensate. The problem is we have no indication from the data itself how much temporal decorrelation has occurred. Hence the required radial scale factor is unknown. However, we can increase the coherence until we secure a first unique solution as intersection with a height/extinction curve. This will occur first for zero extinction but will then also be valid for a whole family of increasing extinction values as shown in the double line region of figure 7. This line region will extend out to the unit circle. Hence we conclude that extinction estimation becomes ambiguous in the presence of temporal decorrelation. A sensible regularization strategy is to set the extinction to zero or some other pre-determined value. In the zero extinction case, we resort to the simple sinc function model for volume coherence and the tree height is then simply related to the maximum vegetation bias  $\phi_w$  as shown in figure 8. With the sinc function model, this phase is just half the vegetation height and so the phase/height/extinction estimates in the presence of temporal decorrelation can be calculated as shown in equation 11

$$\text{temporal decorrelation} \Rightarrow \phi = \phi_1, h_v = \frac{2\phi_v}{k_z}, \sigma = 0 \tag{11}$$

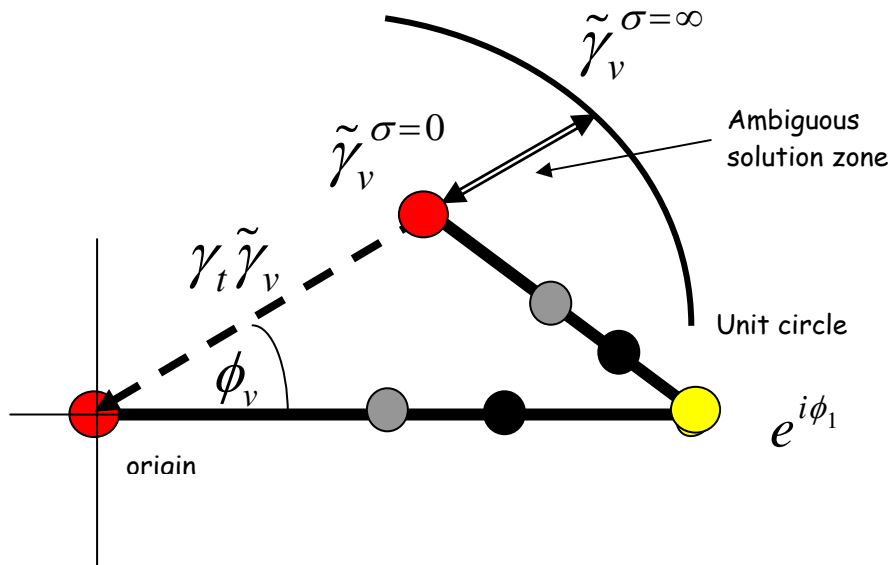


Figure 8 : The effect of temporal decorrelation on the line model

### 1.2.2 The Effect of Vertical Tree structure on Height/Extinction estimation

So far we have assumed a uniform vertical density profile in the vegetation. However natural vegetation has significant species and age related variations in vertical structure. Figure 9 shows an example for Scots Pine trees in the Glen Affric region of Scotland [16]. Here we see tall trees with a high thin canopy. A simple way to model this structure is to add an extra phase parameter to the 2-layer model, essentially making it a three-layer structure. Figure 10 shows a schematic of this new model. The essential modification is to move the canopy away from the ground phase point and this introduces a new phase parameter  $\phi_x$  as shown. With this modification the line model takes the form shown in equation 12.

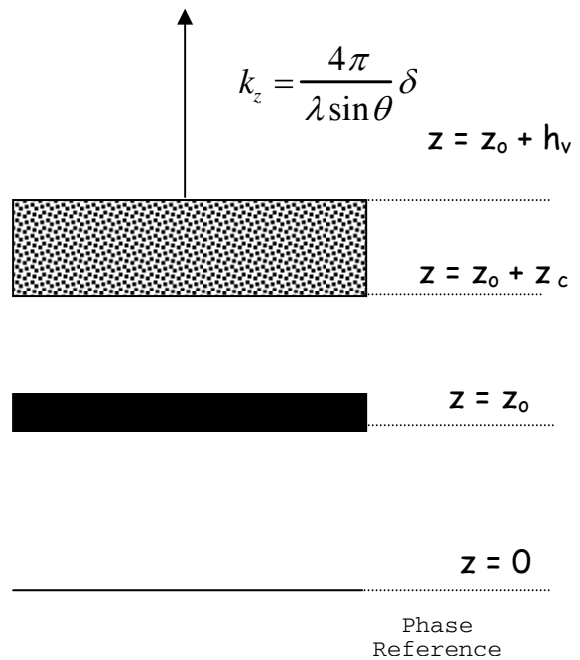


Figure 9 : Vertical tree canopy structure in natural vegetation (Scots Pine) and 3-layer modification of scattering model to account for elevated canopies

$$\tilde{\gamma} = e^{i\phi} \left( e^{i\phi_c} \tilde{\gamma}_v - \frac{\mu}{1+\mu} (1 - e^{i\phi_c} \tilde{\gamma}_v) \right) \quad (12)$$

Geometrically this represents a rotation of the volume coherence point about the origin. Again the line model is still valid but the observed volume coherence is now phase shifted away from its true position. Hence for a given height, the volume coherence is higher than expected based on the simple two-layer model. Nonetheless, this can be accommodated in the model by artificially increasing the extinction. We can see that a fixed coherence can be made to correspond to increasing tree height simply by increasing the extinction. Hence the effect of higher thinner canopies is to increase the extinction estimate with only a small error in the height. For this reason vertical structure is not too serious a limitation for SBPI if only tree height and ground topography are the important parameters of interest. The extinction however becomes an unreliable measure of tree density.

If we have vertical structure combined with temporal decorrelation then equation 11 can overestimate tree height by as much as a factor of 2. In this case only the ground topography estimation becomes a reliable parameter. However, if information is available about the canopy extent of the trees in the scene based on species or age information for example, then equation 11 can be generalized to

$$\text{temporal decorrelation} + \text{canopy fill } F \Rightarrow \phi = \phi_1, \quad h_v = \frac{\phi_v}{k_z(1 - \frac{F}{2})}, \quad \sigma = 0 \quad (13)$$

where  $F = (h_v - z_c)/h_v$  is the fractional canopy fill of the trees.

### 1.2.3 The effect of oriented structure in the volume

We have seen that for POLInSAR remote sensing applications we require there to be significant volume decorrelation. The presence of vegetation causes a loss of coherence and a phase bias. For a single layer of height  $h_v$  and mean extinction  $\sigma$  we have shown that this coherence can be written as shown in equation 14

$$\tilde{\gamma}_v e^{i\phi(z_o)} = \frac{2\sigma e^{i\phi(z_o)}}{\cos \theta_o (e^{2\sigma h_v / \cos \theta_o} - 1)} \int_0^{h_v} e^{ik_z z'} e^{\frac{2\sigma z'}{\cos \theta_o}} dz' \quad (14)$$

However structured volumes, such as agricultural crops and even forests at low frequencies have different extinctions in different polarisations. Hence the volume by itself then requires characterisation by an ordered triplet of coherence values as shown in equation 15.

Equation 15 looks favourable for inversion, as it has four unknown parameters on the right and 6 observations on the left. However, by itself equation 15 is a poor predictor of coherence, as it ignores surface effects and as we have shown, the presence of the soil-air interface beneath the vegetation strongly influences the coherence

$$\sigma_V > \sigma_H \Rightarrow |\tilde{\gamma}_{VV}| > |\tilde{\gamma}_{HV}| > |\tilde{\gamma}_{HH}| \geq 0$$

$$\tilde{\gamma}_{HH} = \frac{2\sigma_H e^{i\phi(z_o)}}{\cos\theta_o (e^{2\sigma_H h_v / \cos\theta_o} - 1)} \int_0^h e^{ik_z z'} e^{\frac{2\sigma_H z'}{\cos\theta_o}} dz'$$

$$\tilde{\gamma}_{HV} = \frac{\sigma_H + \sigma_V e^{i\phi(z_o)}}{\cos\theta_o (e^{(\sigma_H + \sigma_V) h_v / \cos\theta_o} - 1)} \int_0^h e^{ik_z z'} e^{\frac{(\sigma_H + \sigma_V) z'}{\cos\theta_o}} dz'$$

$$\tilde{\gamma}_{VV} = \frac{2\sigma_V e^{i\phi(z_o)}}{\cos\theta_o (e^{2\sigma_V h_v / \cos\theta_o} - 1)} \int_0^h e^{ik_z z'} e^{\frac{2\sigma_V z'}{\cos\theta_o}} dz' \quad (15)$$

To progress we must use the two-layer model, but now modified to account for differential extinction. The general coherence for a vegetation+surface layer may be written as shown in equation 16

$$\tilde{\gamma}_x = e^{i\phi(z_o)} \frac{\gamma_v(k_z, \sigma_a, h_v) + \mu_x}{1 + \mu_x} \quad (16)$$

Here  $\mu$  is the ratio of surface-to-volume scattering and is generally also a function of polarisation ‘x’. Hence equation 15 must be modified to a triplet of such expressions which form the oriented-volume-over-ground or ‘ovog’ model as shown in equation 17

$$\tilde{\gamma}_{HH} = e^{i\phi} \frac{\gamma_v(2\sigma_H, h_v) + \mu_{HH}}{1 + \mu_{HH}}$$

$$\tilde{\gamma}_{HV} = e^{i\phi} \frac{\gamma_v(\sigma_H + \sigma_V, h_v) + \mu_{HV}}{1 + \mu_{HV}}$$

$$\tilde{\gamma}_{VV} = e^{i\phi} \frac{\gamma_v(2\sigma_V, h_v) + \mu_{VV}}{1 + \mu_{VV}} \quad (17)$$

This model now has 7 unknowns on the right and only 6 observations on the left. Hence in the presence of orientation effects we need to fix one parameter for inversion. There are various strategies for the inversion of equation 17 being pursued in the literature, for example we can assume that one of the  $\mu$  values is zero, that the ground phase  $\phi$  is known or as an important special case that the differential extinction is zero in which case we return to our random volume over ground model. Equation 17 has a convenient geometrical representation inside the unit circle of the complex plane. Figure 10 shows this structure. The surface phase  $\phi$  acts as a focus for three rays, representing each of the three primary polarisation combinations. Importantly, the coherence in each polarisation channel is confined to move along its own ray, depending on the value of  $\mu$ . The volume coherences (defined by  $\mu = 0$ ), establish a special triplet of points along the rays as shown. This geometry clearly demonstrates that the biggest error source for unknown orientation effects will be a bias in the ground phase estimate (the three points still almost form a line but intersect the unit circle in the wrong place). This in turn will lead to an underestimation in height.

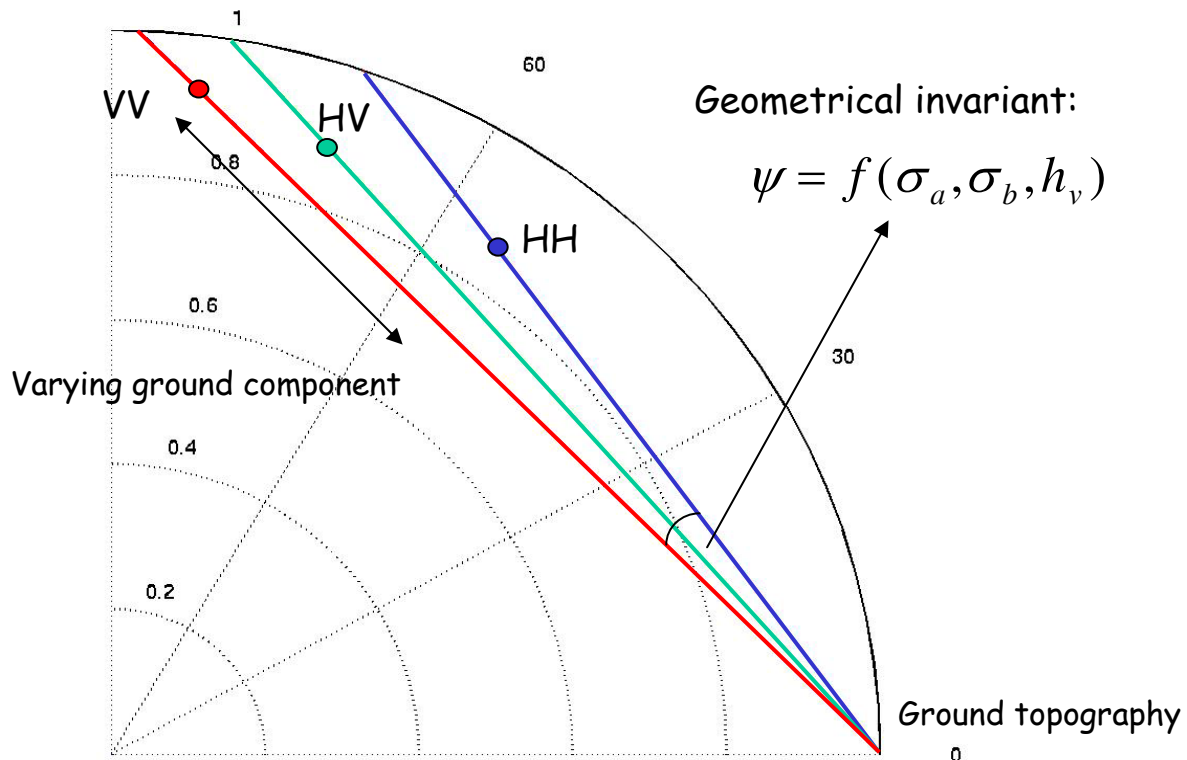


Figure 10 : The geometry of the oriented-volume-over-ground ‘ovog’ model

### 1.3. ALGORITHM ASSESSMENT USING Simulated sar data

In previous publications, validation of these algorithms has been provided using airborne L and P band SAR data across a range of test sites [6,16,19]. These have also addressed the more practical aspects of radar data processing required for operational implementation of these algorithms. Here we concentrate on a different type of validation, involving the use of coherent electromagnetic scattering models. In order to illustrate application of the above algorithm to POLInSAR data, we employ a canopy scattering model with predetermined structure and attempt reconstruction of the height and ground topography from complex coherence data. Note that this model is not the same one used for the algorithm development. To generate a fair test of algorithm performance, a full Maxwell equation based wave propagation and scattering model is used to generate the test data. DSTL Malvern have developed such a capability to model forest scattering in detail, employing a 3-D voxel based vector wave propagation and scattering model tied to a detailed description of branch, leaf and trunk distributions [24,25]. Penetration and scattering are calculated as a function of wavelength and polarisation. The underlying surface scattering is modelled as a tilted Bragg surface and mutual interactions such as ground-trunk and canopy-ground are incorporated in the model. The technique is fully coherent and so can be used to model volume decorrelation effects in polarimetric radar interferometry. The simulated data is free from temporal decorrelation, motion or co-registration errors and SNR effects. Hence we can apply the full inversion scheme to the data as a ‘best case’ scenario.

The SAR simulator was initialised using a point spread function matched to the airborne DLR E-SAR system with 0.69m azimuthal and 1.38m ground range resolution. Simulations were carried out at L-band (23cm wavelength) and at 45 degrees angle of incidence from 3km altitude with 10m and 20m horizontal baselines. These parameters closely match those used for operational E-SAR trials over forest test sites.



A full random canopy ( $F = 1$ ) of 10m height placed above a flat Bragg surface was chosen as the test configuration. The branches chosen to populate the random canopy had dimensions chosen from Gaussian distributions. Branch length had mean 1.5m and standard deviation 0.2m, branch radius had mean 1.5cm and standard deviation 0.2cm. Branch length distribution was truncated at 2.0m and 1.0m, and radii at 1.0cm and 2.0cm. There were 59,153 branches in the canopy with dimensions 56m by 56m by 10m, corresponding to a mean volume fraction of 0.2%. In the simulation branches are further subdivided into smaller elements depending upon the resolution cell size, so that over 200,000 elements existed in the simulation.

Figure 12 shows simulated SAR images of the canopy scene. Note that the canopy scattering appears in all polarization channels, including the cross-polar channel HV. The surface scattering has zero cross polarization but has different scattering components in HH and VV as consistent with the Bragg model. From analysis of the model, the ground contributions beneath the canopy are attenuated by a (one-way) mean extinction of 0.28 dB/m.

We concentrate on a linear azimuth transect through the data as shown. Figure 12 shows sample coherence loci for the point P. Coherence was estimated using a 60-look local boxcar average. In 13 a) we show the interferometric coherence loci for a 10m baseline. Also shown are the least square line fits through the data points. The true ground phase is 0 degrees and we clearly see the vegetation bias in all polarization channels. Note how the line model is a good fit and the intersection point lies close to the true ground phase. In 13 b) we show, for the same test point P, the 20m baseline data for comparison. Here we see a decrease in coherence due to the larger baseline but note that the line fit is still good and unit circle intersect remains close to the true value. Note however the increased variance of coherence estimates, in agreement with equation 9.

In both plots, the HV channel is identified by a circle symbol and we see it has the largest bias as expected from the 2-layer model. We show 5 polarisation states in all, HH, VV, HV, HH+VV and HH-VV. Note that by simply using the phase difference between polarizations we would seriously underestimate the true height. As an example figure 14 shows the estimated height obtained from the phase difference between HH and HV interferometric channels. We see that the average estimate is around 2.5m, well below the true value of 10m. Hence model based corrections are required to obtain better estimates of height. Here we apply the 2-layer model via the geometrical inversion procedure developed above. Figure 15 shows the output from the 3-stage inversion model. Here we show the combined tree height and ground topography estimation for the azimuth transect. We see much improved height estimation and the removal of vegetation bias from the topography estimate.

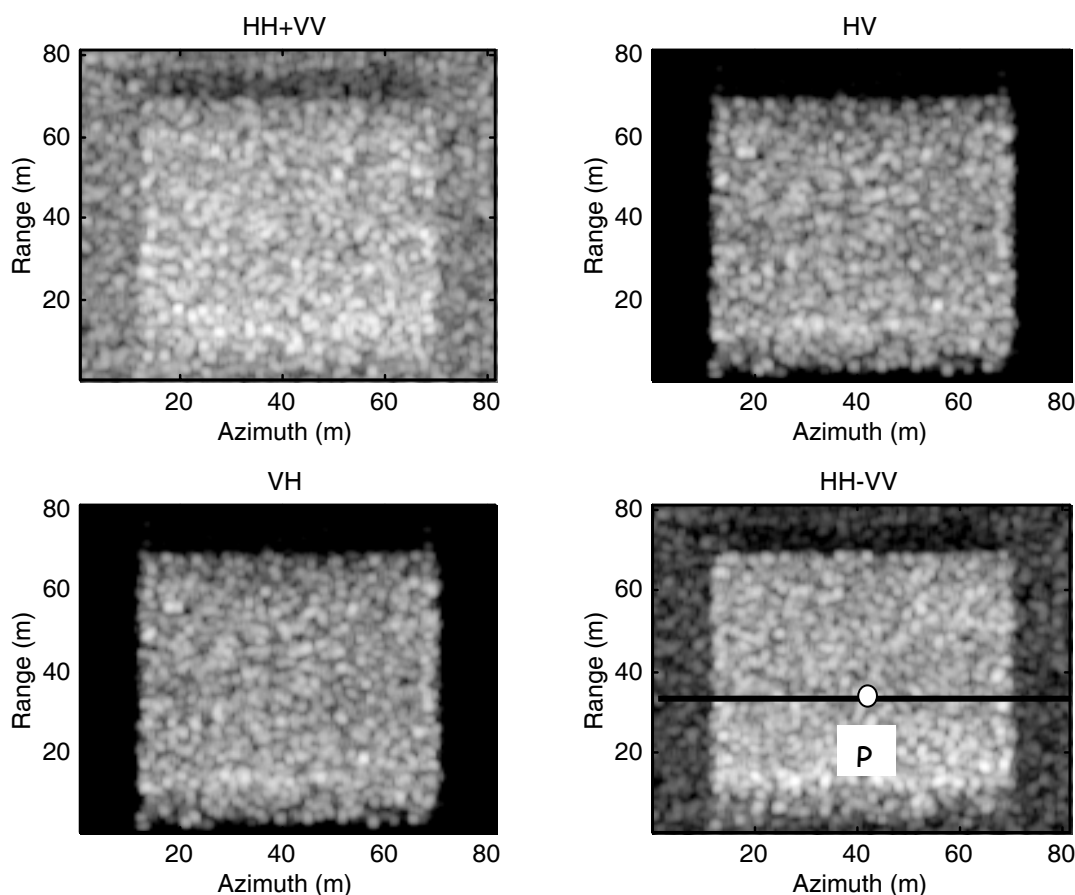


Figure 11 : Simulated L-band SAR images of 10m canopy

Note how the estimates are poor at the edges of the stand, This arises because of the boxcar averaging employed, mixing surface and volume scattering. This causes the local coherence estimates to be low which leads locally to poor parameter estimates. Adaptive edge filtering techniques are being investigated to help resolve this problem [23].

#### 1.4. Conclusions

In this section a simplified 3-stage inversion method was developed for the estimation of underlying ground topography, vegetation height and mean extinction from single baseline polarimetric interferometric SAR data. We have highlighted key potential sources of error in the inversion procedure and shown that to secure good estimates we require one main assumption, namely that in one (not all) of the observed polarization channels, the ground-to-volume scattering ratio is small (less than  $-10\text{dB}$  to secure 10% height accuracy). This highlights the importance of measuring the HV cross-polarized channel for accurate height estimation.

A second key issue is the length of the visible line inside the coherence unit circle. If the line length becomes too short then the inversion becomes unstable. This can arise at very high frequencies, where extinction by vegetation dominates the variation of ground scattering with polarization. However, as long as the visible line length is greater than the complex coherence fluctuations, the line model can be easily extrapolated to find the ground phase point. Hence the technique is inherently robust against the presence or absence of ground-trunk dihedral effects and/or topographic variation. Consequently it can



still provide parameter estimates, even in difficult terrain such as forested slopes where the dihedral return can be attenuated due to topographic variations.

The issue of line visibility can also be used to examine the frequency dependence of the inversion process. Extinction generally increases with frequency and so the line visibility can be expected to decrease as wavelength decreases. However, at very low frequencies the propagation itself can become anisotropic (a function of polarization). In this case the line model is no longer valid, leading to a consequent decrease in parameter accuracy. For these reasons most of our studies have been centred on L-band as a good compromise between the two extremes and because of its well developed technology for air and space borne deployment. However, some initial studies have shown that the technique also applies at P-band for tropical forest environments [19].

The effects of temporal decorrelation, vertical structure and volume orientation on errors in SBPI inversion have been considered and it was shown that in the presence of temporal effects, extinction estimation becomes ambiguous and resort must be made to phase difference algorithms with structure related correction parameters. The effect of vertical structure such as an elevated canopy is to impose a phase transformation on the volume coherence term. This is compensated in the 2-layer model by artificially increasing the extinction. Finally, the effect of orientation in the volume is to split the coherence loci into a fan of three lines centred on the true ground phase. If uncompensated this leads to bias in the ground phase estimate and underestimation of height.

Coherent SAR simulations using the DSTL vector wave scattering model have been used to illustrate the algorithms and demonstrate the need to employ such model based corrections to interferometric phase in order to achieve precision vegetation parameter retrieval. These results clearly demonstrate that tree height and underlying ground topography can be retrieved from a single frequency, single baseline polarimetric sensor. This leads to the possibility of mapping these parameters using air or space borne sensors on regional or even global scales. This is especially important given the close relationship between tree height and biomass [28,29].

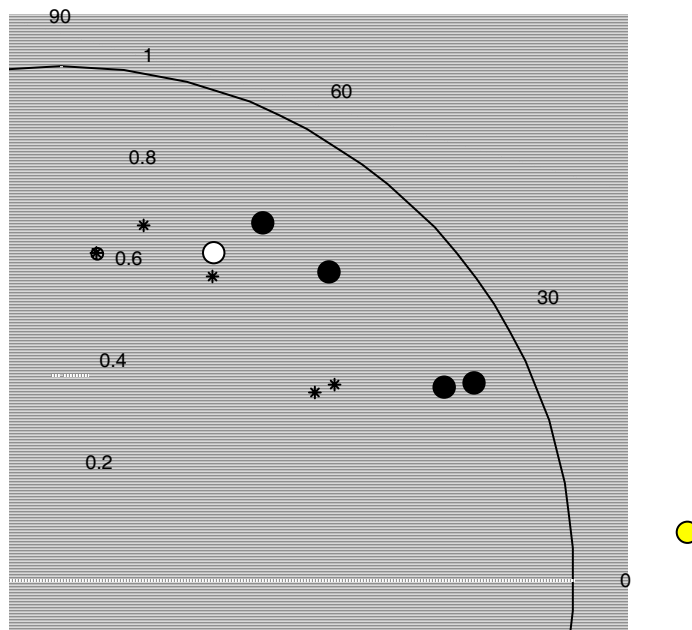
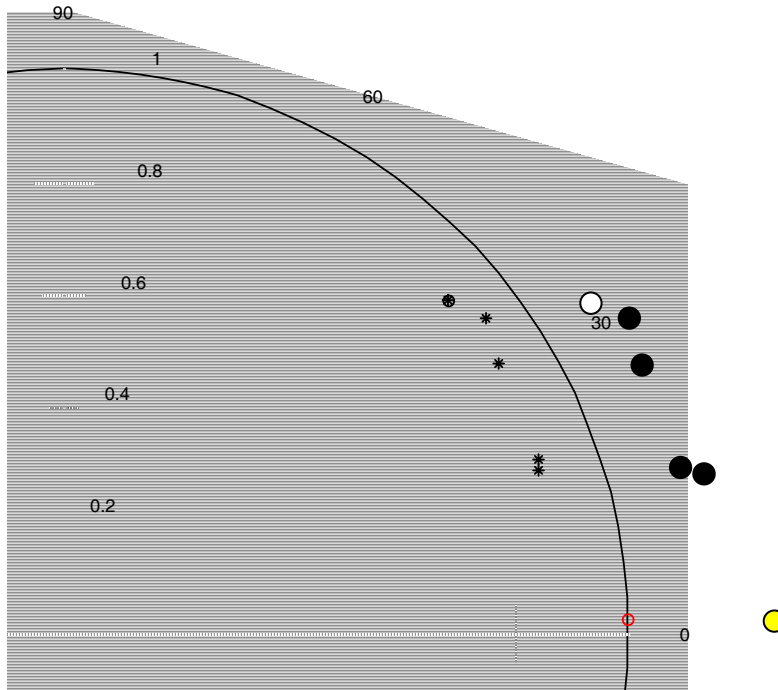


Figure 12 : Sample coherence loci for the point P in figure 12a) 10m baseline b) 20m baseline

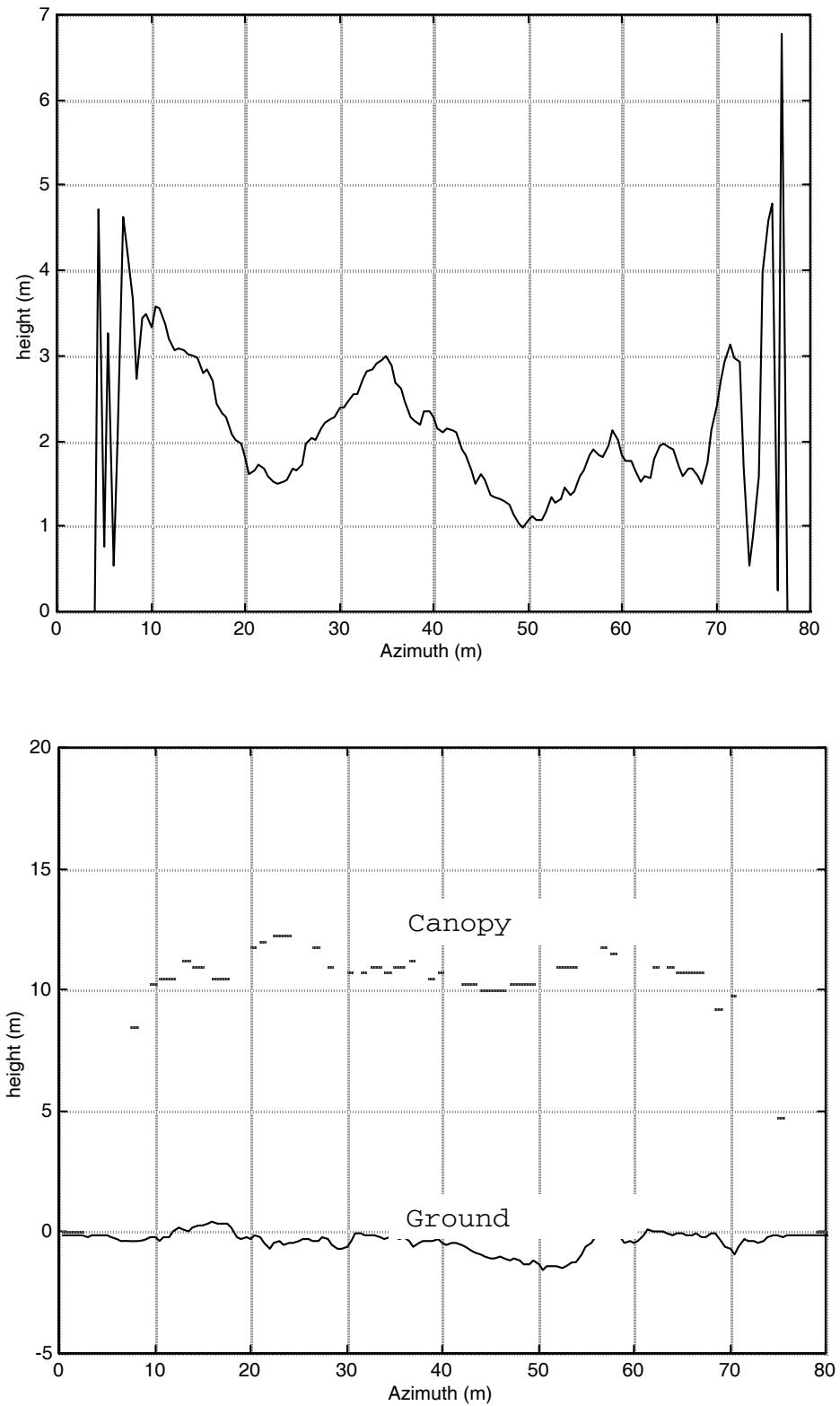


Figure 14 : Tree height estimation based on phase difference between HH and HV interferometric channels (upper) and 3 –stage model inversion (lower)

### Acknowledgements

The work presented here is an excerpt and a summary from the papers of Shane R. Cloude, Douglas Corr and Konstantinos P. Papathanassiou and mainly based on a tutorial given by Shane R. Cloude at EUSAR 2004. Shane R. Cloude and Konstantinos P. Papathanassiou invented and enhanced the concept of polarimetric interferometry within the last couple of years.

### REFERENCES

- [1] CLOUDE S. R., PAPATHANASSIOU K.P., "Polarimetric Optimisation in Radar Interferometry", *Electronics Letters*, Vol. 33, NO. 13, June 1997, pp. 1176-1178
- [2] CLOUDE S. R., PAPATHANASSIOU K.P., "Polarimetric SAR Interferometry", *IEEE Transactions Geoscience and Remote Sensing*, Vol. GRS-36. No. 5, September 1998, pp. 1551-1565
- [3] TREUHAF R. N., MADSEN S., MOGHADDAM M., VAN ZYL J.J., "Vegetation Characteristics and Underlying Topography from Interferometric Data", *Radio Science*, Vol. 31, Dec, 1996, pp. 1449-1495
- [4] TREUHAF R.N., SIQUERIA P., "Vertical Structure of Vegetated Land Surfaces from Interferometric and Polarimetric Radar", *Radio Science*, Vol. 35(1), January 2000, pp 141-177
- [5] LEE J.S., HOPPEL K.W., MANGO S.A., MILLER A., "Intensity and Phase Statistics of Multi-Look Polarimetric and Interferometric SAR Imagery", *IEEE Transactions Geoscience and Remote Sensing*. GE-32, 1994, pp. 1017-1028
- [6] PAPATHANASSIOU K.P., CLOUDE S. R., "Single Baseline Polarimetric SAR Interferometry", *IEEE Transactions Geoscience and Remote Sensing*, Vol 39/11, November 2001, pp 2352-2363
- [7] REIGBER A., MOREIRA A., "First Demonstration of Airborne SAR Tomography Using Multi-Baseline LBand Data", *IEEE Transactions on Geoscience and Remote Sensing*, Vol. 38/5, September 2000, pp 2142-2152
- [8] REIGBER A., "Airborne Polarimetric SAR Tomography", DLR report ISRN DLR-FB-2002-02, 2002
- [9] VAN ZYL J.J., KIM Y., "The Relationship between Radar Polarimetric and Interferometric Phase", *CD Proceedings of IEEE-IGARSS 2000*, Hawaii, USA
- [10] TREUHAF R.N., CLOUDE, S.R., "The Structure of Oriented Vegetation from Polarimetric Interferometry", *IEEE Transactions Geoscience and Remote Sensing*, Vol. 37/2, No. 5, September 1999, pp 2620-2624
- [11] CLOUDE S. R., PAPATHANASSIOU K.P., BOERNER W.M., "The Remote Sensing of Oriented Volume Scattering Using Polarimetric Radar Interferometry", *Proceedings of ISAP 2000*, Fukuoka, Japan, August 2000, pp 549-552
- [12] SEYMOUR S., CUMMING I.G., "Maximum Likelihood Estimation for SAR Interferometry", *Proceedings of IEEE-IGARSS'94*, Pasadena, USA
- [13] TOUZI R., LOPES A., BRUNIQUET J, VACHON P.W., "Coherence Estimation for SAR Imagery", *IEEE Transactions Geoscience and Remote Sensing*, VOL. GRS-37, Jan 1999, pp 135-149
- [14] ISOLA M., CLOUDE, S.R., "Forest Height Mapping using Space Borne Polarimetric SAR Interferometry", *CD Proceedings of IEEE International Geoscience and Remote Sensing Symposium (IGARSS 2001)*, Sydney, Australia, July 2001

- [15] TABB M., CARANDE R., “Robust Inversion of Vegetation Structure Parameters from Low-Frequency, Polarimetric Interferometric SAR”, CD Proceedings of IEEE-IGARSS 2001, Sydney Australia
- [16] CLOUDE S.R., WOODHOUSE I.H., HOPE J., SUAREZ-MINGUEZ J.C., OSBORNE P., WRIGHT G., “The Glen Affric Radar Project: Forest Mapping using dual baseline polarimetric radar interferometry”, Proceedings of Symposium on “Retrieval of Bio and Geophysical Parameters from SAR for Land Applications”, University of Sheffield, England, September 11-14, 2001, ESA publication SP-475, pp 333-338
- [17] ULBRICHT A., FABREGAS X., SAGUES L., “Applying Polarimetric Interferometric Methods to Invert Vegetation Parameters from SAR Data”, CD Proceedings of the IEEE International Geoscience and Remote Sensing Symposium (IGARSS), 9-13 July, Sydney, Australia, 2001
- [18] ULBRICHT A., FRABREGAS X., CASAL M., “Experimental and Theoretical Aspects of Inversion of Polarimetric Interferometric Data”, Proceedings of the Open Symposium on Propagation and Remote Sensing, URSI, Commission F, 12-15 February, Garmisch-Partenkirchen, Germany, 2002
- [19] BRANDFASS M., HOFMANN C., MURA J.C., MOREIRA J., PAPATHANASSIOU K.P., “Parameter estimation of Rain Forest Vegetation via Polarimetric Radar Interferometric Data”, Proceedings of SPIE 2001, Toulouse, France, August 2001
- [20] FLYNN T., TABB M., CARANDE R., “Coherence region Shape Estimation for Vegetation Parameter Estimation in POLINSAR”, Proceedings of IGARSS 2002, Toronto, Canada, pp V 2596-2598
- [21] TABB M., FLYNN T., CARANDE R., “Direct Estimation of Vegetation Parameters from Covariance Data in POLINSAR”, Proceedings of IGARSS 2002, Toronto, Canada, pp III 1908-1910
- [22] YAMADA H., SATO K., YAMAGUCHI Y., BOERNER W.M. “Interferometric Phase and Coherence of Forest Estimated by ESPRIT based POLINSAR”, Proceedings of IGARSS 2002, Toronto, Canada, pp II 832-834
- [23] LEE J.S., CLOUDE S.R., PAPATHANASSIOU K.P., GRUNES M.R., AINSWORTH T., “Speckle Filtering of POLINSAR Data”, Proceedings of IGARSS 2002, Toronto, Canada, pp II 829-831
- [24] WILLIAMS M. L., “Simulating Low Frequency SAR Clutter from a Pine Forest”, Proceedings of 3<sup>rd</sup> European SAR Conference (EUSAR), 23-25 May, 2000, Munich, Germany, pp 149-152
- [25] WILLIAMS M.L., “Prediction and Observation of SAR Clutter from Vegetation Canopies”, Proceedings of IGARSS '99, Hamburg, Germany, pp 1983-1985
- [26] FREEMAN A., DURDEN S.L., “A Three Component Model for Polarimetric SAR Data”, IEEE Transactions on Geoscience and Remote Sensing, Vol. GE-36, 1998, pp. 963-973
- [27] PAPATHANASSIOU K.P., HAJNSEK I., MOREIRA A., CLOUDE S.R., “Forest Parameter Estimation using a Passive Polarimetric Micro-Satellite Concept”, Proceedings of European Conference on Synthetic Aperture Radar, EUSAR'02, pp. 357-360, Cologne, Germany, 4-6 June 2002.
- [28] METTE T., PAPATHANASSIOU K.P., HAJNSEK I., and ZIMMERMANN R., “Forest Biomass Estimation using Polarimetric SAR Interferometry”, Proceedings IGARSS'02 (CD-ROM), Toronto, Canada, 22-26 June 2002

[29] PAPATHANASSIOU K.P., METTE T., HAJNSEK I, KRIEGER G. and MOREIRA A., ‘‘A Passive Polarimetric Micro-Satellite Concept for Global Biomass Mapping’’, Proceedings of the PI-SAR Workshop (CD-ROM), Tokyo, Japan, 29-30 August 2002